

Observationally constrained analysis of sea salt aerosol in the marine atmosphere

Huisheng Bian^{1,2}, Karl Froyd^{3,4}, Daniel M. Murphy³, Jack Dibb⁵, Anton Darmenov², Mian Chin²,
Peter R. Colarco², Arlindo da Silva², Tom L. Kucsera⁶, Gregory Schill^{3,4}, Hongbin Yu², Paul Bui⁷,
Maximilian Dollner⁸, Bernadett Weinzierl⁸, and Alexander Smirnov⁹

¹ University of Maryland at Baltimore County, Baltimore County, MD

² NASA Goddard Space Flight Center, Greenbelt, MD

³ NOAA Earth System Research Laboratory, Chemical Sciences Division, CO

⁴ Cooperative Institute for Research in Environmental Sciences, University of Colorado, Boulder, CO

⁵ University of New Hampshire, Durham, NH

⁶ Universities Space Research Association, Columbia, MD

⁷ NASA Ames Research Center, Moffett Field, CA

⁸ University of Vienna, Faculty of Physics, Aerosol and Environmental Physics, Boltzmanngasse 5, A-1090 Wien, Austria

⁹ Science Systems and Applications, Inc., Lanham, MD 20706

Abstract

Atmospheric sea salt plays important roles in marine cloud formation and atmospheric chemistry. We performed an integrated analysis of NASA GEOS model simulations run with the GOCART aerosol module, *in situ* measurements from the PALMS and SAGA instruments obtained during the NASA ATom campaign, and aerosol optical depth (AOD) measurements from AERONET Marine Aerosol Network (MAN) and from MODIS satellite observations to better constrain sea salt in the marine atmosphere. ATom measurements and GEOS model simulations both show that sea salt

concentrations over the Pacific and Atlantic oceans have a strong vertical gradient, varying up to four orders of magnitude from the marine boundary layer to free troposphere. The modeled residence times suggest that the lifetime of sea salt particles with dry diameter less than 3 μm is largely controlled by wet removal, followed next by turbulent process. During both boreal summer and winter, the GEOS simulated sea salt mass mixing ratios agree with SAGA measurements in the marine boundary layer (MBL) and with PALMS measurements above the MBL. However, comparison of AOD from GEOS with AERONET/MAN and MODIS aerosol retrievals indicated that the model underestimated AOD over the oceans where sea salt dominates. The apparent discrepancy of slightly overpredicted concentration and large underpredicted AOD could not be explained by biases in the model RH affecting the particle hygroscopic growth as modeled RH was found to be comparable to or larger than the in situ measurements. This conundrum could at least partially be explained by the difference in sea salt size distribution; the GEOS simulation has much less sea salt percentage-wise in the smaller particle size range, thus less efficient light extinction, than what was observed by PALMS.

Introduction

Bubble bursting and jet drops at the ocean surface result in the production of sea spray particles composed of inorganic sea salt and organic matter (e.g., de Leeuw et al., 2011; Quinn and Bates, 2013). Among various atmospheric aerosol components, sea salt is estimated to have the largest mass emission flux and the second largest atmospheric mass loading globally (Textor et al., 2006). Sea salt particles in the atmosphere could exert

51 direct radiative effect of around -1.5 to -5.03 W/m² annually at the top of atmosphere
52 (IPCC, 2001). On a global and annual scale, the direct radiative effect of sea salt is equal
53 to or greater in magnitude than that of natural sulfate and soil dust (Jacobson, 2001;
54 Takemura et al., 2002). Sea salt particles are efficient cloud condensation nuclei (CCN).
55 Consequently, sea salt particles have indirect effects on climate and weather
56 (Dadashzaer et al., 2017; Dall et al., 2017, 2018; Kogan et al., 2012; Pierce and Adams,
57 2006). Furthermore, sea salt aerosol particles serve as sinks for reactive gases and small
58 particles and are a source of halogens to the atmosphere (e.g., Alexander et al., 2005;
59 Anastasio et al., 2007; Lawler et al., 2011). There is also observational evidence
60 suggesting that new particle formation may be suppressed in the presence of sea salt
61 aerosol (Browse et al., 2014; Lewis and Schwartz, 2004). To quantify the effects of sea
62 salt aerosol on the environment, a detailed knowledge of its mass, size, and vertical
63 distribution is required. However, measurements of sea salt are not only sparse but also
64 mostly limited to near the surface at a few locations (Prospero et al., 2003), posing
65 difficulties in assessing the global environmental effects of sea salt as well as evaluating
66 model skill at simulating sea salt vertical distributions and properties.

67
68
69 A recent NASA-funded Earth Venture-suborbital project, the Atmospheric Tomography
70 Mission (ATom), deployed an extensive gas and aerosol instrumental payload on the
71 NASA DC-8 aircraft for systematic, global-scale sampling of the atmosphere in four
72 seasons over a 3-year period (2016-2018), profiling continuously from 0.2 to 12 km
73 altitude with flight routes over the Pacific, Atlantic, Southern Ocean, North America and

Greenland from 85°N to 65°S (see Fig. 1). For the first time, vertical profiles of sea salt aerosol concentration and size distribution are measured in ATom over vast oceanic routes in different seasons, providing an unprecedented opportunity for models to evaluate transport and parameterizations of physical and chemical processes.

We present in this study a comprehensive evaluation of sea salt aerosol simulated with the Goddard Chemistry, Aerosol, Radiation, and Transport model (GOCART) in the Goddard Earth Observing System (GEOS) framework using aerosol measurements obtained during the first two ATom deployments, which represent the summer and winter seasons for both hemispheres. We utilize ATom's high frequency vertical measurements of sea salt over global remote oceans from the marine boundary layer (MBL) to the upper troposphere, in contrast with previous model validations of sea salt simulation performed with *in situ* measurements at the surface and over limited selected locations and regions (Chin et al., 2014; Kishcha et al., 2011; Spada et al., 2013, 2015; Tsyro et al., 2011; Witek et al., 2007) and typically using only monthly averaged observations (Grini et al., 2002; Textor et al., 2006). We compare the model simulated sea salt vertical distributions with observations in various latitudinal zones over the Pacific and Atlantic oceans, refer to dry and wet deposition processes, and examine the sea salt size distribution that is important to both AOD calculations and cloud formation.

The GEOS/GOCART model is described in section 2, particularly the sea salt emission scheme used in this study. The NASA ATom field campaign is introduced in section 3, including a brief description of the Particle Analysis by Laser Mass Spectrometry

(PALMS) and Soluble Acidic Gases and Aerosols (SAGA) instruments that are used to provide sea salt measurements. Measured and modeled vertical profiles, size distributions, and AOD are compared to assess model emissions and removal processes in section 4. In section 5, we summarize the outcome of our study and discuss the potentially important chemical/physical processes that likely have an impact on sea salt simulation and recommend future improvements.

Model description

Global aerosol is simulated by GEOS/GOCART, which is a global aerosol model GOCART (Chin et al., 2002, 2014) implemented in the GEOS Earth system model (Gelaro et al., 2017; Rienecker et al., 2011). The GEOS/GOCART aerosols include dust, sea salt, sulfate, nitrate, ammonium, black carbon, and organic matter, mixed externally (Bian et al., 2013; 2017; Colarco et al., 2010).

Sea salt emissions are controlled by aerosol particles generated from collapsing bubbles and ejected jet droplets that in turn are directly related to the whitecap fraction in the ocean and are commonly parameterized as a function of wind speed and SST. The sea salt emission scheme in the GEOS/GOCART model was initially based on the algorithm of Gong (2003) who provided a parameterization of the size-resolved flux of sea salt particles as a function of the 10-m wind speed. Two modifications to this scheme were subsequently developed based on comparisons of simulated sea salt aerosol to satellite AOD from the Moderate Resolution Imaging Spectroradiometer (MODIS) (Darmenov et al., 2013; Randles et al., 2017): 1) the emission function was recalibrated in terms of the

surface friction velocity rather than the 10-m wind speed and 2) a sea surface temperature (SST) correction term that is similar to the work of Jaeglé et al. (2011) was introduced. The model's surface winds are constrained by the two satellite observations, Special Sensor Microwave Imager (SSM/I) and Quick Scatterometer (QuikSCAT) (Rienecker et al., 2011). This emission algorithm is the default GEOS/GOCART sea salt emission and is used in this study.

The current default setting of GEOS/GOCART allows sea salt to be completely removed by warm clouds from convective updraft and from large-scale rainout and washout. Sea salt can also be removed by dry deposition (turbulent) and sedimentation. These processes were described in Chin et al. (2002). We assume that the particles undergo hygroscopic growth according to the equilibrium parameterization of Gerber (1985), which is a function of the relative humidity (RH). The humidified particle sizes are considered in our computations of the particle sedimentation, aerodynamic deposition velocity, and optical properties.

The GEOS/GOCART includes five bulk sea salt size bins in the range of 0.06-20 μm in dry diameter. Specifically, they are 0.06-0.2, 0.2-1.0, 1.0-3.0, 3.0-10, and 10-20 μm , respectively. The first bin was not included in the previous GOCART versions (Chin et al., 2002, 2014), but was added to facilitate aerosol-cloud interactions and optical property studies (Colarco et al. 2010). We further classify the first two bins as fine mode and the remaining bins as coarse mode throughout this paper. The sea salt particle density is 2200 (kg/m^3) for all sizes.

143

144 In this study, we ran GEOS/GOCART at a global ~50 km horizontal resolution on the
145 cubed-sphere grid and 72 vertical layers from surface to 0.01hPa. We ran the model in
146 the “replay” mode, which sets the model dynamical state (winds, pressure, and
147 temperature) at every 6 hours to the balanced state provided by the meteorological
148 reanalysis fields from the Modern-Era Reanalysis for Research and Applications version
149 2 (MERRA-2). An 18 month simulation was conducted from the beginning of 2016 to
150 cover the first two phases of ATom measurement periods, with the first half year as a
151 spin up period.

152

153 **ATom aircraft sea salt measurement from PALMS and SAGA**

154 ATom provides measurements for various important atmospheric gases, aerosols and
155 their precursors over vast open oceans. Among these, sea salt has been measured by two
156 instruments, the NOAA PALMS instrument, which provides mass mixing ratio and size
157 distribution up to 3 μm in dry diameter, and the University of New Hampshire SAGA
158 instrument, which includes measurements of sodium ion (Na^+) as a proxy of sea salt.

159 PALMS is a laser ionization mass spectrometer which makes *in situ* measurements of the
160 chemical composition of individual aerosol particles. A detailed description of PALMS,
161 including its physical working mechanism and measurement features, has been given by
162 Murphy et al., (2019) and Froyd et al., (2019). The instrument is capable of measuring
163 particles from 0.12 to 3 μm in dry diameter and analysis is completed in less than 1
164 millisecond after the aerosols enter the inlet. The real power of the PALMS sea salt
165 measurements is twofold: a) high sensitivity at low concentrations above the MBL such

that the measured vertical profiles are more reliable than most previous data, and b) the data are size-segregated up to 3 μm in dry diameter, covering the active size range for optical and radiative calculations.

On the other hand, the sea salt aerosol mass concentration from SAGA is deduced by applying a factor of 3.27 to the measured Na^+ mass concentration (Keene et al., 1986; Wilson, 1975). This assumes that all of the measured Na^+ comes from sea salt, which should be a reasonable assumption for most ATom samples. SAGA collects particles on a filter with a sampling frequency of around 5-15 minutes to allow more time for the filter media to collect sufficient particles. As reported by the DC-8 Inlet Characterization Experiment (DICE), the SAGA inlet performed nearly identically in the marine boundary environment to the U. Hawaii inlet used by PALMS during ATom (McNaughton et al., 2007). In other words, the cut-off size of the SAGA instrument is also roughly 3 μm in dry diameter. As shown in Murphy et al. (2019), sea salt concentrations inferred from the SAGA sodium data are highly correlated with PALMS sea salt data in the cloud-free MBL.

We use ATom1 (Jul.-Aug., 2016) and ATom2 (Jan.-Feb., 2017) campaign data in this study. These two deployments combined together provided detailed information for summer and winter on a global scale.

Results and Discussions

4.1 Comparisons in the marine boundary layer

189 Sea salt is sufficiently rich in the MBL that SAGA can collect enough aerosol there for
190 analysis. Comparisons of the sea salt in a layer from surface up to 1.5 km between the
191 model simulation and ATom (PALMS and SAGA) measurements are shown in Fig. 2a.
192 To have a proper comparison, we made three data treatments. First, we excluded SAGA
193 samples with significant dust signal, identified when the measurements meet the two
194 conditions: Ca^{2+} greater than $0.05 \mu\text{g}/\text{sm}^3$ and the ratio of Ca^{2+} to Na^+ greater than 0.06.
195 Second, we only include GEOS sea salt particles smaller than $3 \mu\text{m}$ in dry diameter in
196 order to be consistent with the instrument measurements. Third, we sampled GEOS and
197 PALMS data at the SAGA measurement time frequency when the SAGA has valid
198 measurements. The correlation coefficients (R) between the model and PALMS or
199 SAGA data are generally higher than 0.79 and the covariance (R2) higher than 0.64 in
200 both ATom1 and 2 periods.

201
202 There are outliers on the Figure 2a. Just a small amount of cloud can wash off salt
203 previously deposited on an inlet wall. Therefore, in Figure 2b we excluded samples that
204 might be contaminated by clouds during sampling, using a cloud indicator from the
205 Cloud, Aerosol, and Precipitation Spectrometer (CAPS). The outliers are gone on Figure
206 2b and the correlation coefficients between model and measurements are indeed
207 improved from 0.82-0.84 to 0.85-0.87. On the other hand, the GEOS sea salt mass mixing
208 ratios are still more than double of those of PALMS (2.3 in ATom1 and 4.7 in ATom2),
209 which could be at least partially explained by potential sampling biases in PALMS
210 instrument, particularly in the size distribution. The cut-off at $3 \mu\text{m}$ in dry diameter is
211 recommended by the instrument teams, it is known that this is subject to a large

uncertainty of wet/dry size ratio that is strongly dependent on ambient relative humidity. Furthermore, the sea salt mass distribution is (sometimes) still rising sharply through the inlet cutpoints. Considering the combination of all these systematic and random uncertainties, which are decreased across the sea salt coarse mode, the measurement can easily result in uncertainties on the order of $\sim 2\times$ in dry mass. When checking the comparison between GEOS and SAGA, GEOS sea salt mixing ratio is comparable to or slightly larger than SAGA results (i.e. ratio of GEOS to SAGA is 0.92 in ATom1 and 1.3 in ATom2). Overall, the GEOS is most likely to overestimate sea salt mass during February. Comparing sea salt between the two instruments directly shows a high correlation (0.81 in ATom1 and 0.94 in ATom2) as well (also see Murphy et al., 2019).

4.2 Vertical distribution

Understanding the sea salt vertical distribution is important, particularly in the tropical marine upper troposphere where a reliable background aerosol field is needed. However, most previous sea salt measurements were limited to the surface or near coastal areas, leading to nearly no *in situ* observations of the vertical distribution of sea salt over vast areas of the open oceans. The ATom measurements fill this gap by providing measurements over the Pacific, Atlantic, and Southern oceans from near surface to the upper troposphere (0.2-12 km). Furthermore, the PALMS instrument measures *in situ* sea salt mass and size distribution. The high sensitivity of the PALMS instrument makes its data very useful in studying the relatively clean environments above the MBL. Using the ATom sea salt measurements over remote open oceans has some additional advantages over previous studies. For instance, airborne measurements alleviate biases typical at land

stations due to onshore wave breaking activities, especially at sites with steep topography (Witek et al., 2007; Spada et al., 2015).

Figure 3 shows the sea salt vertical profiles of PALMS measurement and GEOS model simulation over 5 latitudinal zones over Pacific and Atlantic oceans in ATom1 and ATom2. The GEOS model results are sampled at the time and location closest to the measurement points. As discussed in section 4.1, modeled sea salt mass concentrations are higher than the PALMS data near the surface over all latitudinal zones during both summer and winter seasons.

There are often two vertical regimes: a sharp gradient of sea salt in the lower atmosphere and a lesser gradient above. Wet removal processes, particularly convective cloud removal, are likely the driving factors for the sea salt distribution in the size range considered in this study (Table 1 column 2). Sea salt is a highly soluble species. It is assumed to fully dissolve in clouds, resulting in efficient removal by shallow marine clouds, typically marine stratus and stratocumulus clouds (Eastman et al., 2011, Lebsock et al., 2011, Wood 2012, Zhou et al., 2015). Sea salt dry deposition (turbulent) and sedimentation also contribute to its removal from low altitudes. Interestingly, the sedimentation process plays the smallest removal role for the sea salt particles with diameter less than 3 μm , whereas it overwhelmingly controls sea salt loss rate (i.e. more than 1.5 times those of all other processes combined) when coarser mode sea salt is included (see Table 1 column 3). This is expected because nearly 90% of injected sea salt mass is in coarse mode based on our emission scheme. Since sea salt is found mostly in

the lower atmosphere, further removal of sea salt particles by cold clouds was found to have only marginal impact on its mass budget in our sensitivity studies, although its feedback on cold clouds needs further study. Note that results in Table 1 are summarized on an annual basis from July 2016 to June 2017.

Atmospheric convection impacts the sea salt vertical distribution as well. The height of the turnaround level (or the transition layer) between two vertical distribution regimes in Fig. 3 is around 600 hPa in the polar regions and moves up to 400 hPa in the tropical region, given that more vigorous convective activities occur in the tropical region. The seasonal variation of the vertical gradient is larger in polar regions than in tropical region, consistent with stronger seasonal variations of the meteorological fields (e.g. T, RH, wind, etc) in high latitudes.

4.3 Marine aerosol AOD

To provide an overall picture of sea salt for this study, we compared the GEOS AOD with satellite MODIS Collection 6 (C6) Aerosol AOD retrieval (Levy et al., 2013) and AERONET Maritime Aerosol Network (MAN) measurements (Smirnov et al., 2017) focusing on sea salt dominated regions. AOD integrates extinction by all aerosols in the atmospheric column, with extinction dependent on the absolute mass, size distribution, hygroscopic growth, vertical distribution, and optical property of each individual component and the composition of aerosols.

Figure 4 shows total AOD comparison between MODIS and GEOS in August 2016 and February 2017. Here, the GEOS AODs are sampled using daily MODIS AOD retrieval. The AODs are only shown where the fraction of sea salt AOD relative to the total aerosol AOD simulated by GEOS (fSSAOD, bottom panel) is larger than 0.6 so that we can focus our discussion over sea salt dominant regions. MODIS AODs are much higher than GEOS AODs for both seasons over remote oceans where sea salt dominates, by 0.043 in August 2016 and 0.062 in February 2017. These differences between MODIS and GEOS are higher than the potential positive bias of MODIS C6 AOD, up to 0.03, over oceans (Figure 16 in Levy et al., 2013). It is difficult for us to remove the MODIS bias in the comparison shown in the Figure 4 since the study of Levy et al., (2013) gave only statistic value of MODIS AOD bias without the information of geophysical location.

The conclusion of a lower GEOS AOD can also be found in Fig. 5 by comparing AOD between ground-based shipboard measurements and the GEOS simulations. AERONET MAN provides ship-borne aerosol optical depth measurements from Microtops II sun photometers. The MAN data is not found to have the positive systematic bias reported for MODIS. MAN measurements from July, 2016 to June 2017 are used in this study. The GEOS model results are sampled at the closest time and location of the ship-based measurements. The model AODs are much smaller than MAN measurements over a majority of the open ocean areas except part of the Atlantic Ocean where AOD was impacted by dust. The scatter plot at the bottom of the figure indicates clearly that the modeled AOD is biased low, especially over the Southern Ocean where the model AOD is less than half of MAN's.

303

304 On the one hand, GEOS's sea salt mass is comparable to SAGA *in situ* measurements in
305 the MBL, and on the other hand, GEOS underestimates AOD when compared with
306 measurements from MAN and MODIS. The agreement with PALMS vertical gradients
307 shows that the AOD cannot be explained by sea salt above the MBL. There are various
308 potential reasons for this conundrum, such as the sea salt size distribution, atmospheric
309 relative humidity, sea salt particle hygroscopic growth rate, sea salt refractive index, etc.
310 We will discuss the first two potential reasons below.

311

312 **4.4 Size distribution and atmospheric RH**

313 The sea salt size distribution is a key factor in AOD calculation because small particles
314 are more optically efficient at light extinction. Aerosol size also modulates the transport
315 and removal processes. The necessity to study sea salt size distribution lies also in the
316 important role of sea salt particle sizes that affects atmospheric chemistry, radiative
317 effects, and cloud formation processes.

318

319 To compare the sea salt size distributions between the model and ATom data, we
320 calculate normalized percentage of sea salt mass in each of the first three size bins for
321 PALMS and GEOS over three atmospheric vertical layers for ATom1 and 2, as shown in
322 Figure 6. The three vertical layers (i.e. 0-1.5, 1.5-6, and >6 km) represent the boundary
323 layer, middle troposphere, and upper troposphere. GEOS sea salt particle mass and size
324 have been computed at RH of 45% to match the measurement condition of PALMS. The
325 particle sizes here are limited to be less than 3 μm in dry diameter due to the size cut of

the PALMS inlet. Particles in this range are most important in light extinction and cloud formation with many more sea salt particles in fine mode than in coarse mode on a per unit mass basis.

Figure 6 reveals that the size distribution is more flat in PALMS than in GEOS. In other words, with the same sea salt mass, the fraction of sea salt in the finest mode in PALMS is much larger (i.e. about 5-7 times higher) than in GEOS. To quantify the potential impact of sea salt size distribution on AOD calculation, we calculate the sea salt mass extinction efficiency (MEE) integrated over the three bins using the two size distributions of PALMS and GEOS at RH 45% and 550 nm in the same three vertical layers and in the whole atmosphere (Table 2). The size segregated MEEs used in the calculation are 1.6, 5.6, and 1.2 m² g⁻¹ for the bins 1-3, respectively. The effective MEE from GEOS for the size range is 1.7 m² g⁻¹, which is about 24% lower than 2.2 m² g⁻¹ calculated with the PALMS size distribution. Thus, the underestimation of GEOS AOD shown in Figure 5c may partially stem from the model underestimate of the small sea salt particles, especially for those with diameter less than 1 μm (Figure 6). The underestimation of AOD by GEOS is more significant in the boundary layer shown in Table 2, which implies that the sea salt size distribution from emission may need to be revisited.

Apparently, sea salt size distribution is a potential culprit for the dichotomy in GEOS simulation since GEOS partitions more sea salt onto larger particles that are less optically active compared with the significant fine sea salt mode observed in PALMS measurements. Such large underestimation of fine sea salt particles by the model may

349 have significant implications not only on the AOD calculation but also on studies of
350 radiative effects and cloud formation because particle number concentration is a key
351 quantity for these processes. The conclusion that GEOS sea salt size distribution favors
352 the coarse mode sea salt particles is consistent with a recent study of Naumann et al.,
353 (2016), which found that the sea salt emission of Gong (2003) yielded overestimations in
354 the PM10 measured at coastal stations and underestimations at inland stations over
355 northwestern Europe.

356
357 Sea salt particle size distribution changes horizontally and vertically, but the change is
358 much smaller than the difference between those of model and measurement. This implies
359 a possibility of using a global size distribution without sacrificing much accuracy.

360
361 Another possible contribution to underestimation of the AOD due to sea salt in the model
362 is if there is a general underestimate in the humidification of sea salt particles in the
363 model, with a corresponding underestimate on optical efficiency per unit dry mass.

364 Figure 7 compares atmospheric RHs between ATom measurements and GEOS
365 simulations along flight tracks summarized over the same regions as in Fig. 3. With only
366 a few exceptions, the model RH is higher than the ATom measurements, including in the
367 MBL, where humidity is typically high. Thus, atmospheric water vapor simulation is not
368 responsible for the low AOD calculation. In fact, using measured RH along with the
369 model's sea salt size distribution and vertical distribution would give even lower AOD.

370 There should be other factors contributing to a lower GEOS AOD calculation as well,
371 such as sea salt hygroscopic growth rate, sea salt optical properties, and other aerosol

species over ocean. Further investigations for these factors are needed to better understand the GEOS sea salt simulation.

Conclusions

A systematic and comprehensive global sea salt study was conducted by integrating NASA GEOS model simulations with ATom *in situ* measurements from the PALMS and SAGA instruments, as well as AOD measurements from AERONET MAN and satellite MODIS over the oceans. This work takes advantage of PALMS sea salt vertical profile measurement together with SAGA filter measurements in MBL, covering global remote regions over the Pacific, Atlantic, and Southern Oceans from near the surface to ~12 km altitude and in both summer and winter seasons. Important atmospheric sea salt fields, e.g. mass mixing ratio, vertical distribution, size distribution, and aerosol AOD, are examined. The meteorological field of RH and the sea salt simulation processes of emission, dry deposition, sedimentation, and large scale and convective wet depositions were explored to explain the sea salt fields and to reveal a potential direction for model improvement.

Generally, the agreement between ATom measurements and the model is remarkable, both in terms of absolute loading and especially in the shape of the vertical distribution under a wide range of different tropospheric environments. The correlation coefficients are generally higher than 0.8 between GEOS-PALMS and GEOS-SAGA for both ATom1 and ATom2 periods. GEOS results capture the strong sea salt vertical gradient shown in the measurements except over SH high latitudes, where the PALMS's gradient is deeper.

In the MBL, the current GEOS sea salt simulation is comparable (ATom1) or slightly higher (ATom2) than SAGA data, which in turn is higher than PALMS data.

An underestimation of GEOS aerosol AOD over sea salt dominated oceans is found from the comparison of AODs between GEOS and MAN, as well as GEOS and MODIS. This is contradictory to the finding that GEOS sea salt mass abundance is comparable to or slightly higher than measurements. This conundrum may be partially attributed to the difference in sea salt mass size distributions between GEOS and PALMS. The GEOS sea salt mass size distribution favors the coarse mode while PALMS has a larger fraction of more optically active submicron sea salt. The atmospheric water vapor, however, can be ruled out as the cause of model underestimation of AOD, since the GEOS RH is comparable to or higher than ATom measurements almost everywhere along the flight tracks, especially in MBL.

Atmospheric sea salt vertical distribution is impacted by various processes including emission, hygroscopic growth, dry deposition, sedimentation, wet deposition, convection, and large-scale advection. Among these processes, wet deposition, owing to both shallow marine cloud structure and rapid hygroscopic growth of sea salt particles, is most important in shaping the vertical profile for the size range studied in this work and results in a sharp gradient in the low atmosphere where RH is typically very high. Vertical convection is also important for explaining the sea salt vertical profiles.

More work is needed in the future to investigate sea salt hygroscopic growth rate, optical properties, sea water salinity, sea ice, and marine organic aerosol to understand the dilemma in GEOS simulation. Consideration of variations in salinity of surface seawater is missing in the GEOS aerosol model. Although salinity may not be an important factor in sea salt emission on the global scale owing to its relatively uniformity across the world oceans, it may be important regionally as discussed by Grythe et al., (2014). Salinity also impacts sea spray aerosol (SSA) size. The dry SSA size distribution shifts towards smaller sizes with lower salinities found in the EMEP intensive campaigns (Barthel et al., 2014). Sea ice, whose contribution is also neglected in the GEOS aerosol model, could be an important source of sea salt aerosol over polar regions and has significant implications for polar climate and atmospheric chemistry reported by recent publications (Dall et al., 2017; May et al., 2016; Rhodes et al., 2017). More importantly, primary marine organic aerosols (Randles et al., 2004), which come also from sea spray bubble bursting as sea salts but are more submicron particles, should be investigated to disentangle the sea spray aerosols.

Author contribution

Huisheng Bian and Mian Chin designed the experiments. Peter R. Colarco, Anton Darmanov, Arlindo da Silva, Tom L. Kucsera, and Hongbin Yu contributed to GEOS-GOCART model setup and provided tools to analyze model data. Huisheng Bian conducted the model simulation and in charge of the analyses. Karl Froyd, Daniel M. Murphy, and Gregory Schill provided ATom PALMS measurement data. Jack Dibb provided ATom SAGA measurement data. Maximilian Dollner and Bernadett Weinzierl provided ATom CAPS cloud data. Paul Bui provided ATom MMS data for RH measurement. Hongbin Yu and Alexander Smirnov provided MODIS satellite

and AERONET MAN measurement data. All authors contributed to the data analyses and paper writing.

Acknowledgments

This research was supported by two programs of the National Aeronautics and Space Administration (NASA): Atmospheric Composition: Modeling and Analysis Program (ACMAP) and Earth Venture-suborbital program for the Atmospheric Tomography Mission (ATom).

References:

- Alexander, B., R. J. Park, D. J. Jacob, Q. B. Li, R. M. Yantosca, J. Savarino, C. C. W. Lee, and M. H. Thiemens (2005), Sulfate formation in sea-salt aerosols: Constraints from oxygen isotopes, *J. Geophys. Res.*, 110, D10307, doi:10.1029/2004JD005659.
- Anastasio, C. and Newberg, J. T.: Sources and sinks of hydroxyl radical in sea-salt particles, *J. Geophys. Res.*, 112, D10306, doi:10.1029/2006JD008061, 2007.
- Barthel, S., Tegen, I., Wolke, R., and van Pinxteren, M.: Model study on the dependence of primary marine aerosol emission on the sea surface temperature, *Atmos. Chem. Phys. Discuss.*, 14, 377-434, <https://doi.org/10.5194/acpd-14-377-2014>, 2014.
- Bian, H., Chin, M., Hauglustaine, D. A., Schulz, M., Myhre, G., Bauer, S. E., Lund, M. T., Karydis, V. A., Kucsera, T. L., Pan, X., Pozzer, A., Skeie, R. B., Steenrod, S. D., Sudo, K., Tsigaridis, K., Tsimpidi, A. P., and Tsyro, S. G.: Investigation of global nitrate from the

465 AeroCom Phase III experiment, *Atmos. Chem. Phys.*, 17, 12911-12940,
466 <https://doi.org/10.5194/acp-17-12911-2017>, 2017.

467 Bian, H., P. Colarco, M. Chin, G. Chen, J.M. Rodriguez, Q. Liang, et al., Investigation of source
468 attributions of pollution to the Western Arctic during the NASA ARCTAS field campaign.
469 *Atmos. Chem. and Phys.*, 13, 4707-4721, doi:10.5194/acp-13-4707-2013, 2013.

470 Browse, J., Carslaw, K. S., Mann, G. W., Birch, C. E., Arnold, S. R., and Leck, C.: The complex
471 response of Arctic aerosol to sea-ice retreat, *Atmos. Chem. Phys.*, 14, 7543-7557,
472 <https://doi.org/10.5194/acp-14-7543-2014>, 2014.

473 Chin, M., T. Diehl, Q. Tian, J. M. Prospero, R. A. Kahn, A. Remer, H. Yu, A. M. Sayer, H. Bian,
474 et al., Multi-decadal variations of atmospheric aerosols from 1980 to 2009: sources and regional
475 trends, *Atmos. Chem. Phys.*, 14, 3657-3690, doi:10.5194/acp-14-3657-2014, 2014.

476 Chin, M., P. Ginoux, S. Kinne, B. N. Holben, B. N. Duncan, R. V. Martin, J. A. Logan, A.
477 Higurashi, and T. Nakajima, 2002: Tropospheric aerosol optical thickness from the GOCART
478 model and comparisons with satellite and sun photometer measurements, *J. Atmos. Sci.* 59, 461-
479 483.

480 Colarco, P., da Silva, A., Chin, M., and Diehl, T.: On- line simulations of global aerosol
481 distributions in the NASA GEOS-4 model and comparisons to satellite and ground based aerosol
482 optical depth, *J. Geophys. Res.*, 115, D14207, doi:10.1029/2009JD012820, 2010.

483 Dadashazar, H., Wang, Z., Crosbie, E., Brunke, M., Zeng, X., Jonsson, H., Woods, R. K., Flagan,
484 R. C., Seinfeld, J. H., and Sorooshian, A.: Relationships between giant sea salt particles and
485 clouds inferred from aircraft physico-chemical data, *J. Geophys. Res.-Atmos.*, 122, 3421–3434,
486 <https://doi.org/10.1002/2016JD026019>, 2017.

487 Dall'Osto, M., Geels, C., Beddows, D.C.S., Boertmann, D., Lange, R., Nøjgaard, J.K., Harrison
488 Roy, M., Simo, R., Skov, H., Massling, A., 2018. Regions of open water and melting sea ice drive
489 new particle formation in North East Greenland. *Sci. Rep.* 8,6109.

490 Dall'Osto, M., Beddows, D.C.S., Tunved, P., Krejci, R., Ström, J., Hansson, H.-C., Yoon, Y.J.,
 491 Park, Ki-Tae, Becagli, S., Udisti, R., Onasch, T., O'Dowd, C.D., Simó, R., Harrison, Roy M.,
 492 2017a. Arctic sea ice melt leads to atmospheric new particle formation. 2017. Scientific Reports
 493 7, P. 3318. <https://doi.org/10.1038/s41598-017-03328-1>.
 494 Darmanov, A., da Silva, A., Liu, X. and Colarco, P. R., (2013), Data-driven aerosol development
 495 in the GEOS-5 modeling and data assimilation system, Abstract A43D-0305 presented at 2013
 496 Fall Meeting, AGU, San Francisco, Calif., 9-13 Dec.
 497 de Leeuw, G., Andreas, E. L., Anguelova, M. D., Fairall, C.W., Lewis, E. R., O'Dowd, C., Schulz,
 498 M., and Schwartz, S. E.: Production flux of sea spray aerosol, Rev Geophys, 49, RG2001,
 499 doi:10.1029/2010rg000349, 2011.
 500 Eastman, R., S. G. Warren, and C. J. Hahn, 2011: Variations in cloud cover and cloud types over
 501 the ocean from surface observations, 1954–2008. J. Climate, 24, 5914–5934.
 502 Froyd, K. D., Murphy, D. M., Brock, C. A., Campuzano-Jost, P., Dibb, J. E., Jimenez, J.-L.,
 503 Kupc, A., Middlebrook, A. M., Schill, G. P., Thornhill, K. L., Williamson, C. J., Wilson, J. C.,
 504 and Ziemba, L. D.: A new method to quantify mineral dust and other aerosol species from aircraft
 505 platforms using single particle mass spectrometry, Atmos. Meas. Tech. Discuss.,
 506 <https://doi.org/10.5194/amt-2019-165>, in review, 2019.
 507 Gelaro, R., McCarty, W., Suárez, M. J., Todling, R., Molod, A., Takacs, L., Randles, C. A.,
 508 Darmanov, A., Bosilovich, M. G., Reichle, R., Wargan, K., Coy, L., Cullather, R., Draper, C.,
 509 Akella, S., Buchard, V., Conaty, A., da Silva, A. M., Gu, W., Kim, G. K., Koster, R., Lucchesi,
 510 R., Merkova, D., Nielsen, J. E., Partyka, G., Pawson, S., Putman, W., Rienecker, M., Schubert, S.
 511 D., Sienkiewicz, M., and Zhao, B.: The Modern-Era Retrospective Analysis for Research and
 512 Applications, Version 2 (MERRA-2), J. Climate, 30, 5419–5454, [https://doi.org/10.1175/JCLI-D-](https://doi.org/10.1175/JCLI-D-16-0758.1)
 513 16-0758.1, 2017.
 514 Gerber, H. E. (1985), Relative-humidity parameterization of the Navy aerosol model (NAM),
 515 NRL Rep. 8956, Naval Res. Lab., Washington, D. C.

516 Grini, A., M. Myhre, J. K. Sundet, and I. S. A. Isaksen, Modeling the Annual Cycle of Sea Salt
 517 in the Global 3D Model Oslo CTM2: Concentrations, Fluxes, and Radiative Impact, *Journal of*
 518 *Climate*, 15(13), 1717–1730. [https://doi.org/10.1175/1520-0442\(2002\)](https://doi.org/10.1175/1520-0442(2002)).
 519 Gong, S. L., A parameterization of sea-salt aerosol source function for sub- and super-micron
 520 particles, *Global Biogeochem. Cycles*, 17 (4), 1097, doi:10.1029/2003GB002079, 2003.
 521 Grythe, H., Ström, J., Krejci, R., Quinn, P., and Stohl, A.: A review of sea-spray aerosol source
 522 functions using a large global set of sea salt aerosol concentration measurements, *Atmos. Chem.*
 523 *Phys.*, 14, 1277-1297, <https://doi.org/10.5194/acp-14-1277-2014>, 2014.
 524 Intergovernmental Panel on Climate Change (IPCC) 2001 In *Climate Change 2001: The*
 525 *Scientific Basis* (eds J. T. Houghton, Y. Ding, D. J. Griggs, M. Noguer, P. J. van der Linden and
 526 D. Xiaosu), New York, NY: Cambridge University Press.
 527 Jacobson, M. Z. (2001), Global direct radiative forcing due to multicomponent anthropogenic and
 528 natural aerosols, *J. Geophys. Res.*, 106(D2), 1551-1568.
 529 Jaeglé, L., Quinn, P. K., Bates, T. S., Alexander, B., and Lin, J.-T.: Global distribution of sea salt
 530 aerosols: new constraints from insitu and remote sensing observations, *Atmos. Chem. Phys.*, 11,
 531 3137–3157, doi:10.5194/acp-11-3137-2011, 2011.
 532 Kogan, Yefim L., David B. Mechem, Kityan Choi, Effects of Sea-Salt Aerosols on Precipitation
 533 in Simulations of Shallow Cumulus, <https://doi.org/10.1175/JAS-D-11-031.1>, 2012.
 534 Keene W. C., Psxenny A. A. P., Galloway J. N. and Hawley M. E. (1986) Seasalt corrections and
 535 interpretation of constituent ratios in marine precipitation. *J. Geophys. RES.* 91,6647-6658.
 536 Kishcha, P., Nickovic, S., Starobinetes, B., di Sarra, A., Udisti, R., Becagli, S., Sferlazzo, D.,
 537 Bommarito, C., Alpert, P., 2011. Sea-salt aerosol forecasts compared with daily measurements at
 538 the island of Lampedusa (Central Mediterranean). *Atmospheric Research* 100, 28-35.
 539 Lawler, M. J., Sander, R., Carpenter, L. J., Lee, J. D., von Glasow, R., Sommariva, R., and
 540 Saltzman, E. S.: HOCl and Cl₂ observations in marine air, *Atmos. Chem. Phys.*, 11, 7617-7628,
 541 <https://doi.org/10.5194/acp-11-7617-2011>, 2011.

542 Lebsock MD, L'Ecuyer TS, Stephens GL (2011) Detecting the ratio of rain and cloud water in
 543 low-latitude shallow marine clouds. *J Appl Meteorol Climatol* 50:419-432.
 544 <https://doi.org/10.1175/2010JAMC2494.1>.
 545 Levy, R. C., Mattoo, S., Munchak, L. A., Remer, L. A., Sayer, A. M., Patadia, F., and Hsu, N. C.:
 546 The Collection 6 MODIS aerosol products over land and ocean, *Atmos. Meas. Tech.*, 6, 2989-
 547 3034, <https://doi.org/10.5194/amt-6-2989-2013>, 2013.
 548 Lewis, E.R., Schwartz, S.E., 2004. Sea salt aerosol production: mechanisms, methods,
 549 measurements and models - a critical review. *Geophysical Monograph*, vol. 152. Print
 550 ISBN:9780875904177 |Online ISBN:9781118666050 |DOI:10.1029/GM152, American
 551 Geophysical Union, Washington, DC.
 552 May, N. W., Quinn, P. K., McNamara, S. M., and Pratt, K. A.: Multiyear study of the dependence
 553 of sea salt aerosol on wind speed and sea ice conditions in the coastal Arctic, *J. Geophys. Res.* -
 554 *Atmos.*, 121, 9208–9219, <https://doi.org/10.1002/2016JD025273>, 2016.
 555 McNaughton, C. S., Clarke, A. D., Howell, S. G., Pinkerton, M., Anderson, B., Thornhill, L.,
 556 Hudgins, C., Winstead, E., Dibb, J. E., Scheuer, E., and Maring, H.: Results from the DC-8 Inlet
 557 Characterization Experiment (DICE): Airborne Versus Surface Sampling of Mineral Dust and
 558 Sea Salt Aerosols, *Aerosol. Sci. Tech.*, 41, 136–159, 2007.
 559 Murphy, D. M., Froyd, K. D., Bian, H., Brock, C. A., Dibb, J. E., DiGangi, J. P., Diskin, G.,
 560 Dollner, M., Kupc, A., Scheuer, E. M., Schill, G. P., Weinzierl, B., Williamson, C. J., and Yu, P.:
 561 The distribution of sea-salt aerosol in the global troposphere, *Atmos. Chem. Phys.*, 19, 4093-
 562 4104, <https://doi.org/10.5194/acp-19-4093-2019>, 2019.
 563 Neumann, D., Matthias, V., Bieser, J., Aulinger, A., and Quante, M.: A comparison of sea salt
 564 emission parameterizations in north-western Europe using a chemistry transport model setup,
 565 *Atmos. Chem. Phys.*, 16, 9905–9933, doi:10.5194/acp-16-9905-2016, 2016.

566 Pierce, J. R., and P. J. Adams (2006), Global evaluation of CCN formation by direct emission of
 567 sea salt and growth of ultrafine sea salt, *J. Geophys. Res.*, 111, D06203,
 568 doi:10.1029/2005JD006186.
 569 Quinn PK and TS Bates, *Ocean-Derived Aerosol and Its Climate Impacts*, 5.12, Published by
 570 Elsevier Ltd., 2013.
 571 Prospero, J. M., Savoie, D. L., and Arimoto, R.: Long-term record of nss-sulfate and nitrate in
 572 aerosols on Midway Island, 1981–2000: evidence of increased (now decreasing?) anthropogenic
 573 emissions from Asia, *J. Geophys. Res.*, 108, 4019, doi:10.1029/2001JD001524, 2003.
 574
 575 Randles, C. A., Russell, L. M., and Ramaswamy, V.: Hygroscopic and optical properties of
 576 organic sea salt aerosol and consequences for climate forcing, *Geophys. Res. Lett.*, 31, L16 108,
 577 doi:10.1029/2004GL020628, 2004.
 578 Randles, C. A., da Silva, A. M., Buchard, V., Colarco, P. R., Darmenov, A., Govindaraju, R.,
 579 Smirnov, A., Holben, B., Ferrare, R., Hair, J., Shinozuka, Y., and Flynn, C. J.: The MERRA-2
 580 Aerosol Reanalysis, 1980-onward, Part I: System Description and Data Assimilation Evaluation,
 581 *J. Climate*, 30, 6823–6850, <https://doi.org/10.1175/jcli-d-16-0609.1>, 2017.
 582 Rhodes, R. H., Yang, X., Wolff, E. W., McConnell, J. R., and Frey, M. M.: Sea ice as a source of
 583 sea salt aerosol to Greenland ice cores: a model-based study, *Atmos. Chem. Phys.*, 17, 9417–
 584 9433, <https://doi.org/10.5194/acp-17-9417-2017>, 2017.
 585 Rienecker, M. M., Suarez, M. J., Gelaro, R., Todling, R., Bacmeister, J., Liu, E., Bosilovich, M.
 586 G., Schubert, S. D., Takacs, L., Kim, G. K., Bloom, S., Chen, J., Collins, D., Conaty, A., da Silva,
 587 A., Gu, W., Joiner, J., Koster, R. D., Lucchesi, Andrea Molod, A., Owens, T., Pawson, S.,
 588 Pegion, P., Redder, C. R., Reichle, R., Robertson, F. R., Ruddick, A. G., Sienkiewicz, M., and
 589 Woollen, J.: MERRA: NASA’s Modern-Era Retrospective Analysis for Research and
 590 Applications, *J. Climate*, 24, 3624–3648, 2011.

591 Smirnov, A., M. Petrenko, C. Ichoku, and B. Holben. 2017. "Maritime Aerosol Network optical
 592 depth measurements and comparison with satellite retrievals from various different sensors."
 593 Remote Sensing of Clouds and the Atmosphere XXII, [10.1117/12.2277113].
 594 Spada, M., Jorba, O., Pérez García-Pando, C., Janjic, Z., and Baldasano, J. M.: Modeling and
 595 evaluation of the global sea-salt aerosol distribution: sensitivity to size-resolved and sea-surface
 596 temperature dependent emission schemes, *Atmos. Chem. Phys.*, 13, 11735-11755,
 597 <https://doi.org/10.5194/acp-13-11735-2013>, 2013.
 598 Spada, M., Jorba, O., Pérez García-Pando, C., Janjic, Z., and Baldasano, J. M.: On the evaluation
 599 of global sea-salt aerosol models at coastal/orographic sites, *Atmos. Environ.*, 101, 41–48,
 600 <https://doi.org/10.1016/j.atmosenv.2014.11.019>, 2015
 601 Takemura, T., Nakajima, T., Dubovik, O., Holben, B. N., and Kinne, S.: Single-scattering albedo
 602 and radiative forcing of various aerosol species with a global three-dimensional model, *J.*
 603 *Climate*, 15(4), 333–352, 2002
 604 Textor, C., Schulz, M., Guibert, S., Kinne, S., Balkanski, Y., Bauer, S., Berntsen, T., Berglen, T.,
 605 Boucher, O., Chin, M., Dentener, F., Diehl, T., Easter, R., Feichter, H., Fillmore, D., Ghan, S.,
 606 Ginoux, P., Gong, S., Grini, A., Hendricks, J., Horowitz, L., Huang, P., Isaksen, I., Iversen, I.,
 607 Kloster, S., Koch, D., Kirkevåg, A., Kristjansson, J. E., Krol, M., Lauer, A., Lamarque, J. F., Liu,
 608 X., Montanaro, V., Myhre, G., Penner, J., Pitari, G., Reddy, S., Seland, Ø., Stier, P., Takemura,
 609 T., and Tie, X.: Analysis and quantification of the diversities of aerosol life cycles within
 610 AeroCom, *Atmos. Chem. Phys.*, 6, 1777–1813, <https://doi.org/10.5194/acp-6-1777-2006>, 2006.
 611 Tsyro, S., W. Aas, J. Soares, M. Sofiev, H. Berge, and G. Spindler, Modelling of sea salt
 612 concentrations over Europe: key uncertainties and comparison with observations, *Atmos. Chem.*
 613 *Phys.*, 11, 10367–10388, 2011, www.atmos-chem-phys.net/11/10367/2011/, doi:10.5194/acp-11-
 614 10367-2011.
 615 Wilson, T. R. S., Salinity and the major elements of sea water, in *Chemical Oceanography*, vol. 1,
 616 2nd ed., edited by J.P. Riley and G. Skirrow, pp. 365-413, Academic, Orlando, Fla., 1975.

Witek, M. L., P. J. Flatau, P. K. Quinn, and D. L. Westphal, 2007: Global sea-salt modeling: Results and validation against multicampaign shipboard measurements. *J. Geophys. Res.*, 112, D08215, doi:10.1029/2006JD007779.

Wood, R., 2012. Stratocumulus clouds. *Month. Weath. Rev.* 140, 2373–2423.

Zhou, X., Kollias, P., & Lewis, E. R. (2015). Clouds, precipitation, and marine boundary layer structure during the MAGIC field campaign. *Journal of Climate*, 28(6), 2420–2442. <https://doi.org/10.1175/JCLI-D-14-00320.1>.

Table 1. Sea salt (SS) budget analysis on annual basis from July 2016 to June 2017 (the 2th column: GEOS SS up to 3 μm in dry diameters, the 3th column: GEOS SS for all bins, and the 4th column AeroCom SS for all bins).

	GEOS SS ($\text{Dp}^a < 3\mu\text{m}$)	GEOS SS (all bins)	AeroCom SS (all bins)
Emission (Tg/yr)	515.2	4015.5	2190-117949
Burden (Tg)	1.63	6.80	3.4-18.2
Lifetime (days)	1.16	0.62	0.03-1.59
Surf concentration ($\mu\text{g/kg}$)	3.2	16.5	
Dry deposition (Tg/yr)	103.1	460.9	
Sedimentation (Tg/yr)	61.1	2458.2	
Kdry^b (days^{-1})	1.17	1.17	0.06-2.94
LS^c deposition (Tg/yr)	140.3	354.7	
SV^d deposition (Tg/yr)	211.8	746.1	
Kwet^e (days^{-1})	0.44	0.44	0.11-2.45
$\text{SSAOD}_{550\text{nm}}$		0.0269	0.003-0.067

^a Dp : particle diameter (μm)

^b Kdry : loss frequency due to dry deposition and sedimentation (days^{-1})

^c LS : large scale wet deposition (Tg/yr)

^d SV : convective wet deposition (Tg/yr)

^e Kwet : loss frequency due to wet large scale and convective depositions (days^{-1})

Table 2. Sea salt mass extinction efficient (MEE) for PALMS and GEOS and the ratio of MEEs between GEOS and PALMS in three vertical layers and in the whole atmosphere at RH 45%

	PALMS (m^2/kg)	GEOS (m^2/kg)	R(GEOS/PALMS) %
0 – 1.5 KM	2636.87	1618.09	61.4
1.5 – 6 KM	2089.97	1671.61	80.0
>6 KM	1891.07	1786.24	94.5
all	2203.67	1679.36	76.2

642

643 **Figure Captions**

644 **Figure 1.** AToM1 (top) and AToM2 (bottom) flight track sorted out for each flight day.

645

646 **Figure 2a.** Scatter plot of sea salt between GEOS and PALMS (magenta) and between
647 GEOS and SAGA (blue) in AToM1 (symbol +) and AToM2 (symbol \diamond) for all flight
648 measurements within 1.5 km atmospheric thickness above ocean surface. The SAGA
649 samples are filtered out when dust signal is significant. The GEOS sea salt shown here
650 are cut at 3 μm in dry diameters. Both GEOS and PALMS data are then sampled using
651 SAGA measurement time frequency. The statistical parameter r is the correlation
652 coefficient and b is the ratio of $\text{SS}(\text{GEOS})$ to $\text{SS}(\text{ATom})$.

653

654 **Figure 2b.** Similar to Figure 2a with the samples contaminated by clouds are further
655 excluded using CAPS cloud indicator.

656

657 **Figure 3.** Sea salt ($D_p < 3 \mu\text{m}$) vertical profiles from GEOS simulation and PALMS
658 measurement along AToM1 and 2 flight tracks in 5 latitudinal bands over Pacific and
659 Atlantic oceans. The latitudinal bands are marked by dot grey lines in Figure 1.

660

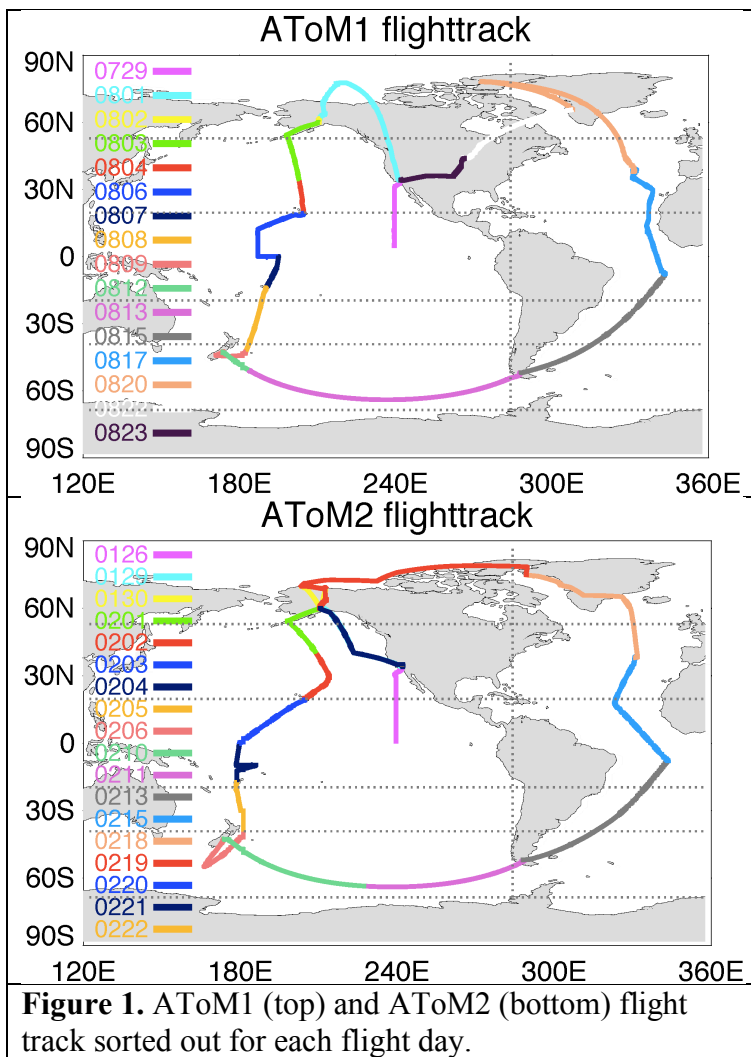
661 **Figure 4.** Total aerosol AOD in 201608 (left column) and 201702 (right column) from
662 MODIS (top) and GEOS (middle). The bottom panel shows the mass fraction of sea salt
663 relative to the total aerosol simulated by GEOS.

664

Figure 5. Total AOD measured by MAN cruise occurred during 201607 to 201706 (5a) and simulated by GEOS but sampled with MAN measurement (5b). 5c shows total AOD scattering plot between MAN and GEOS and the purple color is for the data over Southern Ocean shown inside the boxes in Figure 5b.

Figure 6. Percentage distribution of sea salt mass over the first three bins normalized to the total sea salt with particle wet diameter up to $\sim 5 \mu\text{m}$ at RH 45%. The normalized SS mass weighting distribution is sorted over three vertical layers and for ATom1 (top row) and ATom2 (bottom row), respectively.

Figure 7. Atmospheric RH vertical profiles from GEOS simulation and ATom measurement along ATom1 and 2 flight tracks in 5 latitudinal bands over Pacific and Atlantic oceans.



685
686
687
688
689
690
691
692
693
694
695
696
697
698
699
700
701
702

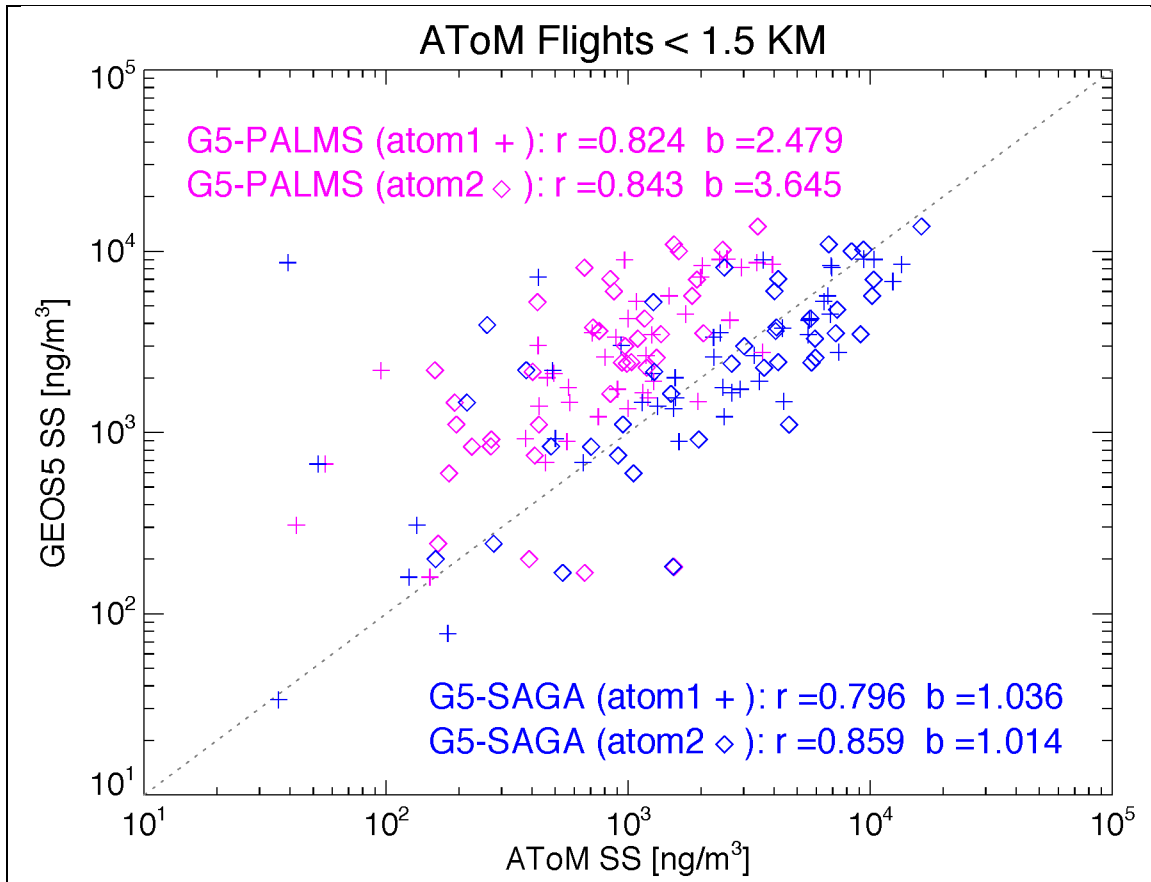
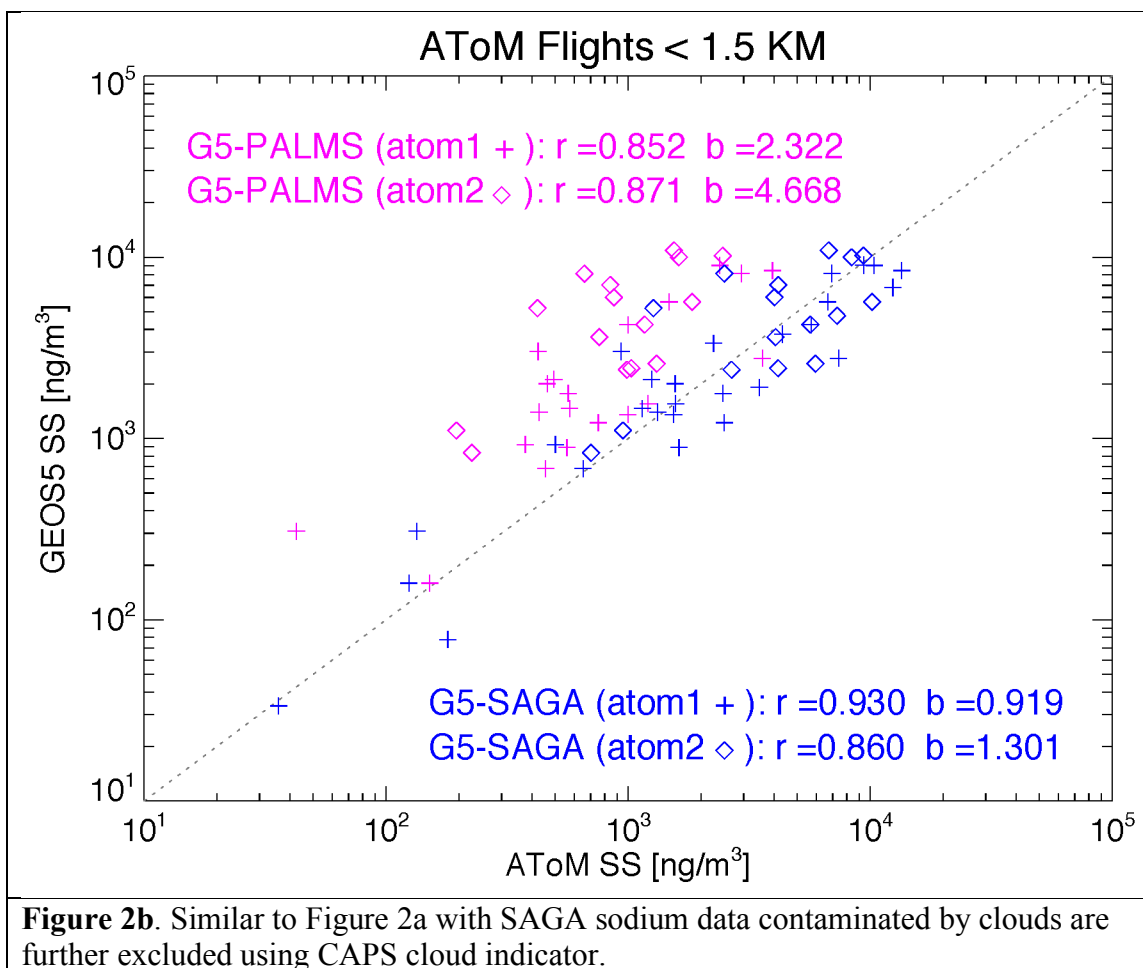


Figure 2a. Scatter plot of sea salt between GEOS and PALMS (magenta) and between GEOS and SAGA (blue) in AToM1 (symbol +) and AToM2 (symbol ◇) for all flight measurements within 1.5 km atmospheric thickness above ocean surface. The SAGA samples are filtered out when dust signal is significant. The GEOS sea salt shown here are cut at 3 μm in dry diameters. Both GEOS and PALMS data are then sampled using SAGA measurement time frequency. The statistical parameter r is the correlation coefficient and b is the ratio of SS(GEOS) to SS(AToM).

703
704
705
706



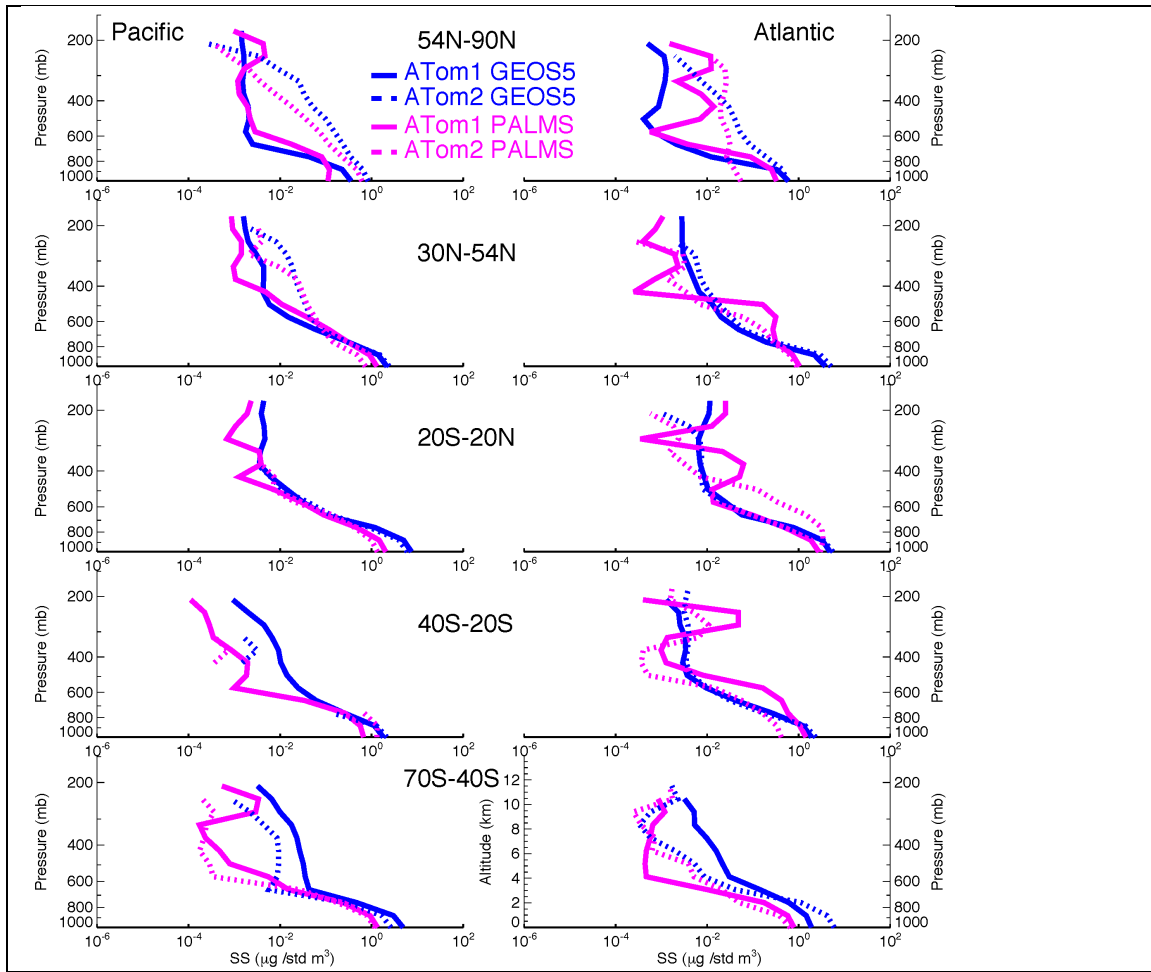


Figure 3. Sea salt ($D_p < 3 \mu\text{m}$) vertical profiles from GEOS5 simulation and PALMS measurement along ATom1 and 2 flight tracks in 5 latitudinal bands over Pacific and Atlantic oceans. The latitudinal bands are marked by dot grey lines in Figure 1.

707
708
709
710
711
712
713
714
715
716
717
718
719
720
721
722

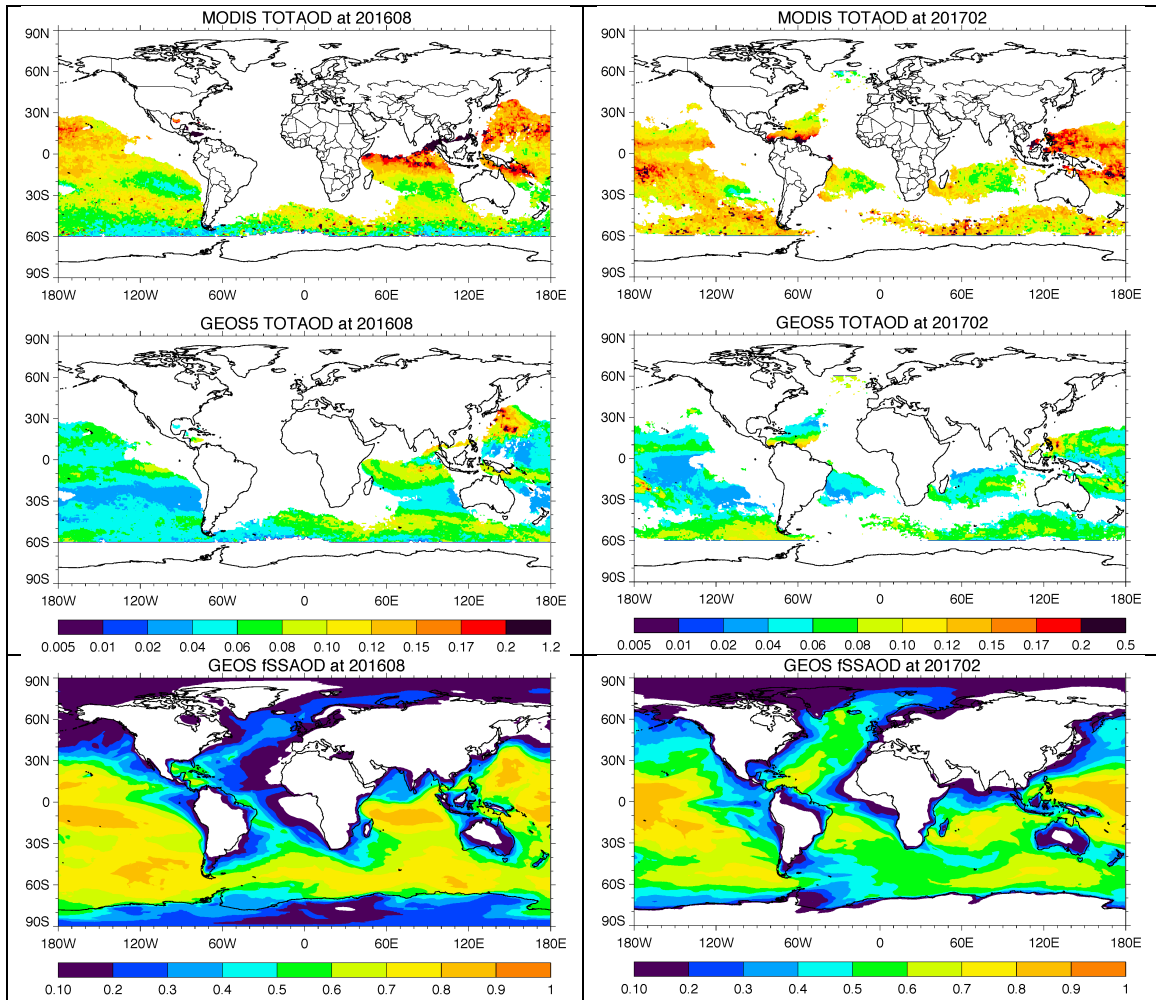


Figure 4. Total aerosol AOD in 201608 (left column) and 201702 (right column) from MODIS (top) and GEOS5 (middle) over oceans where fraction of sea salt AOD (fSSAOD) mass simulated by GEOS (bottom panel) is larger than 0.6.

723
724
725
726
727
728
729
730
731
732
733
734
735
736
737
738

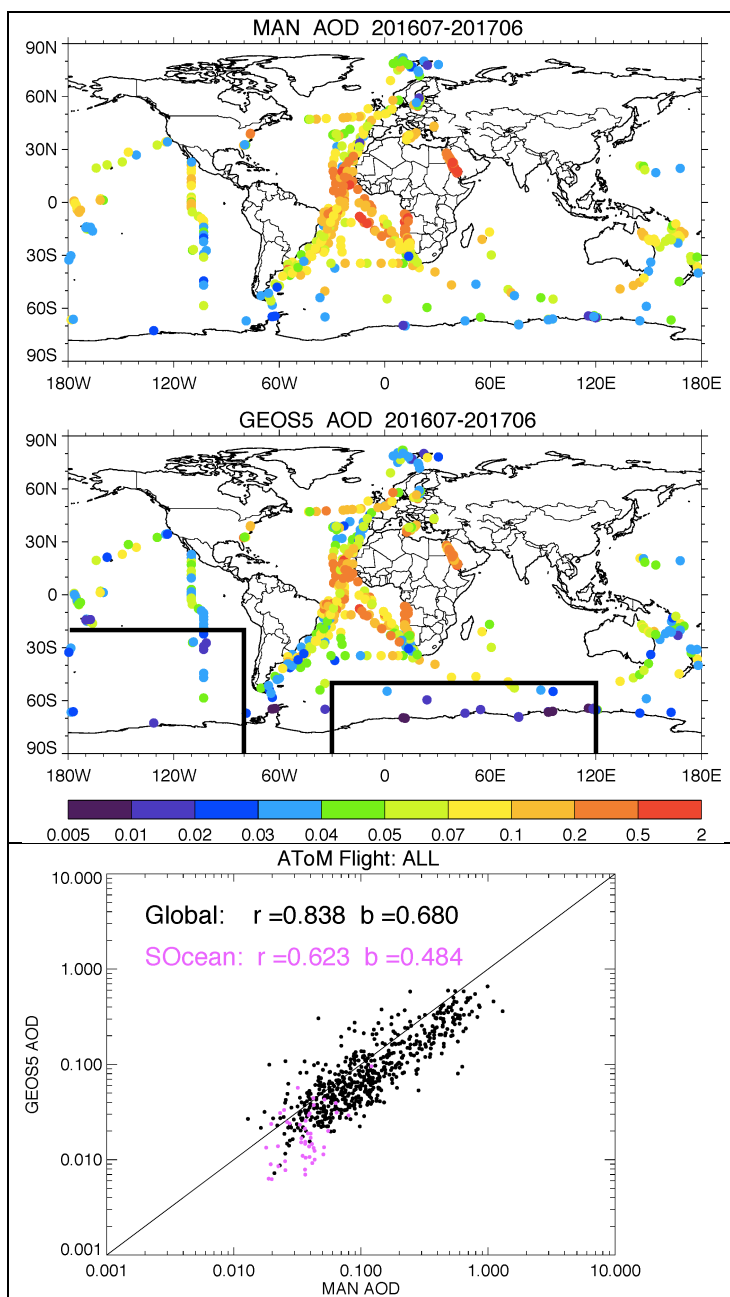


Figure 5. Total AOD measured by MAN cruise occurred during 201607 to 201706 (5a) and simulated by GEOS5 but sampled with MAN measurement (5b). 5c shows total AOD scattering plot between MAN and GEOS and the purple color is for the data over Southern Ocean shown inside the boxes in Figure 5b.

740

741

742

743

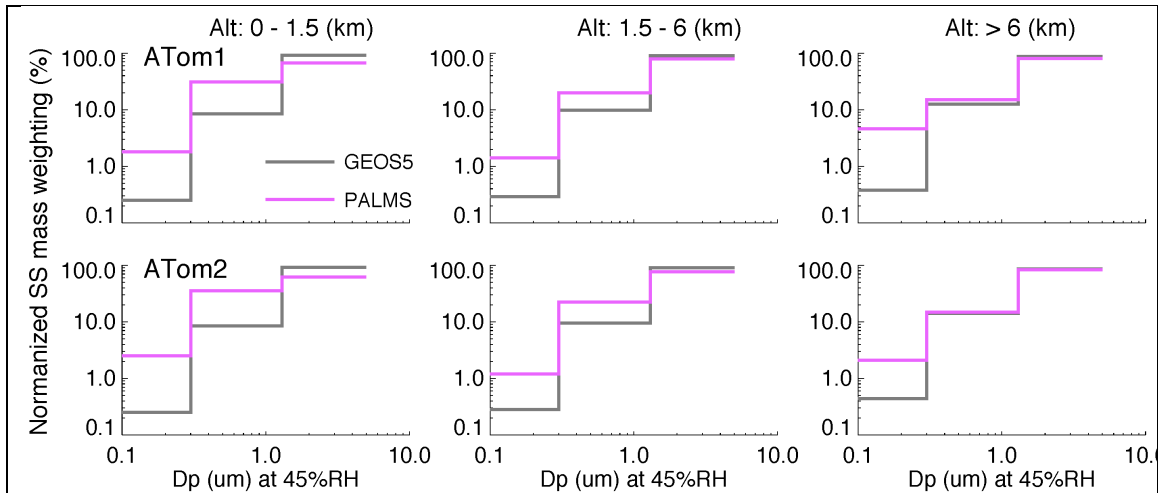


Figure 6. Percentage distribution of sea salt mass over the first three bins normalized to the total sea salt with particle wet diameter up to $\sim 5 \mu\text{m}$ at RH 45%. The normalized SS mass weighting distribution is sorted over three vertical layers and for ATom1 (top row) and ATom2 (bottom row), respectively.

744
745
746
747
748
749
750
751
752
753
754
755

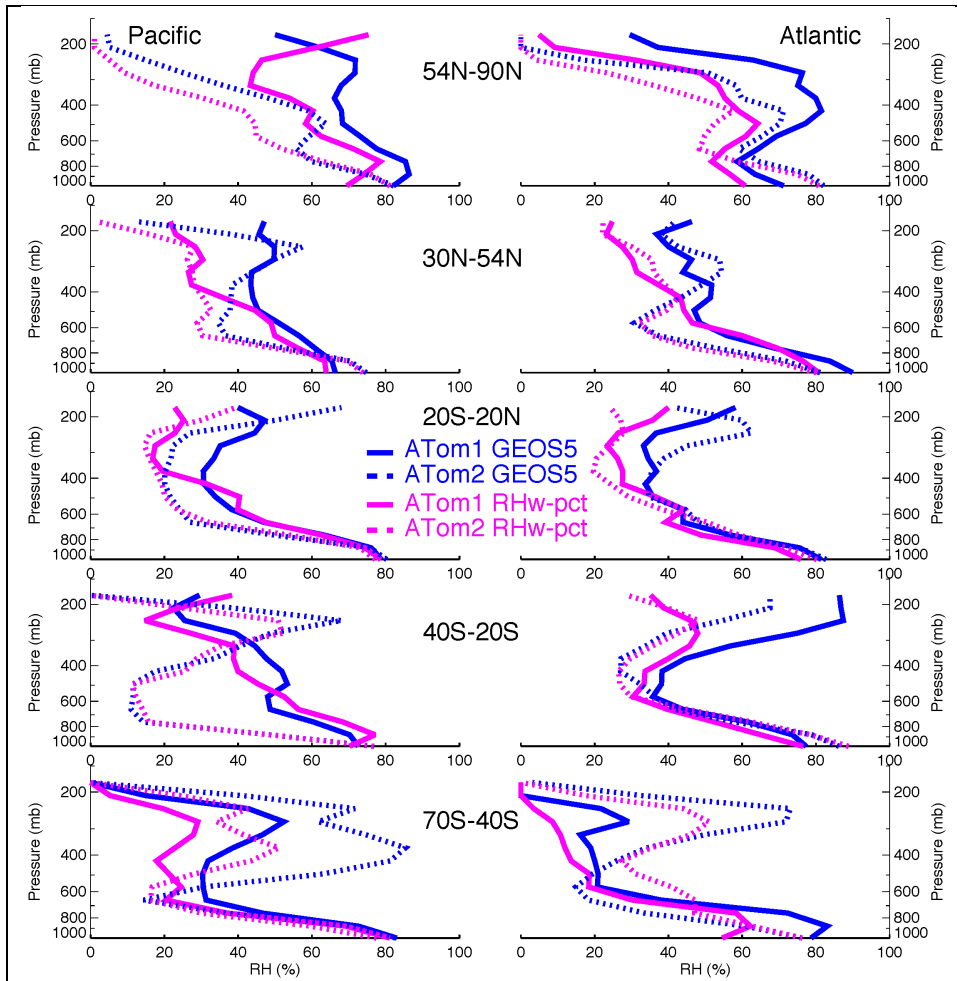


Figure 7. Atmospheric RH vertical profiles from GEOS5 simulation and ATom measurement along ATom1 and 2 flight tracks in 5 latitudinal bands over Pacific and Atlantic oceans.